PLOS ONE

RESEARCH ARTICLE

Combination therapy of cancer with cancer vaccine and immune checkpoint inhibitors: A mathematical model

Xiulan Lai[1]*, **Avner Friedman**[2]

1 Institute for Mathematical Sciences, Renmin University of China, Beijing, P. R. China, **2** Mathematical Biosciences Institute & Department of Mathematics, Ohio State University, Columbus, OH, United States of America

* xiulanlai@ruc.edu.cn

Citation: Lai X, Friedman A (2017) Combination therapy of cancer with cancer vaccine and immune checkpoint inhibitors: A mathematical model. PLoS ONE 12(5): e0178479. https://doi.org/10.1371/journal.pone.0178479

Editor: Nikolas K. Haass, University of Queensland Diamantina Institute, AUSTRALIA

Received: December 19, 2016

Accepted: May 12, 2017

Published: May 25, 2017

Data Availability Statement: All relevant data are within the paper.

Funding: This work is supported by the Mathematical Biosciences Institute and the National Science Foundation (Grant DMS 0931642), and the Renmin University of China and the International Postdoctoral Exchange Fellowship Program 2016 by the Office of China Postdoctoral Council.

Competing interests: The authors have declared that no competing interests exist.

Abstract

In this paper we consider a combination therapy of cancer. One drug is a vaccine which activates dendritic cells so that they induce more T cells to infiltrate the tumor. The other drug is a checkpoint inhibitor, which enables the T cells to remain active against the cancer cells. The two drugs are positively correlated in the sense that an increase in the amount of each drug results in a reduction in the tumor volume. We consider the question whether a treatment with combination of the two drugs at certain levels is preferable to a treatment by one of the drugs alone at 'roughly' twice the dosage level; if that is the case, then we say that there is a positive 'synergy' for this combination of dosages. To address this question, we develop a mathematical model using a system of partial differential equations. The variables include dendritic and cancer cells, $CD4^+$ and $CD8^+$ T cells, IL-12 and IL-2, GM-CSF produced by the vaccine, and a T cell checkpoint inhibitor associated with PD-1. We use the model to explore the efficacy of the two drugs, separately and in combination, and compare the simulations with data from mouse experiments. We next introduce the concept of synergy between the drugs and develop a synergy map which suggests in what proportion to administer the drugs in order to achieve the maximum reduction of tumor volume under the constraint of maximum tolerated dose.

Introduction

When cancer cells undergo necrosis, they release high mobility group box-1 (HMGB-1) which activates dendritic cells [1–3]. Activated dendritic cells (DCs) mature as APC cells and play a critical role in the communication between the innate and adaptive immune responses. Once activated, dendritic cells produce IL-12, which activates effector T cells $CD4^+$ Th1 and $CD8^+$ T [4, 5]. Th1 produces IL-2 which further promotes proliferation of the effector T cells. Both $CD4^+$ Th1 and $CD8^+$ T cells kill cancer cells [6–8]. $CD8^+$ T cells are more effective in killing cancer cells, but the helper function of $CD4^+$ Th1 cells improves the efficacy of tumor-reactive $CD8^+$ T cells [9].

Cancer vaccines serve to enlarge the pool of tumor-specific T cells from the naive repertoire, and also to activate tumor specific T cells which are dormant [10]. GM-CSF can activate dendritic cells, and is commonly used as a cancer vaccine [11–13]. GVAX is a cancer vaccine composed of tumor cells genetically modified to secrete GM-CSF and then irradiated to prevent further cell division.

PD-1 is an immunoinhibitory receptor predominantly expressed on activated T cells [14, 15]. Its ligand PD-L1 is upregulated on the same activated T cells, but it is also expressed by some human cancer cells, such as in melanoma, lung cancer, colon cancer, and leukemia [15–17]. The complex PD-1-PD-L1 is known to inhibit T cell function [14]. Immune checkpoints are regulatory pathways in the immune system that inhibit its active response against specific targets. In the case of cancer, the complex PD-1-PD-L1 forms an immune checkpoint for T cells.

There has been much progress in recent years in developing checkpoint inhibitors, primarily PD-1 antibodies and PD-L1 antibodies [17]. Such drugs have been increasingly explored in single-agent studies for cancer treatment [16, 18]. The FDA recently approved several checkpoint inhibitors. However, because of lack of tumor-infiltrating effector T cells, many patients in clinical trials do not respond to checkpoint inhibitor treatment [18]. On the other hand, cancer vaccines have been shown to induce effector T-cells infiltration into tumors [19], although, to be fully effective, cancer vaccines have to overcome immune evasion [10]. It was recently suggested that the combination of a cancer vaccine and an immune checkpoint inhibitor may function synergistically to induce more effective antitumor immune responses [18, 20]. Clinical trials to test such combination therapies are currently ongoing [18, 20]; mouse experiments are also being conducted [21–27].

In the present paper we develop a mathematical model of treatment of cancer with a cancer vaccine combined with an immune checkpoint inhibitor; specifically, we combine GVAX and PD-1 inhibitor. In order to focus on the combination therapy of the two drugs, we consider in the model only the following variables: cancer cells (C), dendritic cells (DCs), $CD4^+$ and $CD8^+$ T cells, GM-CSF, PD-1, PD-L1, PD-1-PD-L1 complex, and cytokines IL-12 and IL-2. These species interact within the network shown in Fig 1. The mathematical model is based on Fig 1, and it is represented by a system of partial differential equations (PDEs). Simulations of the model are shown to be in qualitative agreement with the mouse experiments reported in [21–23]. The model is then used to explore the efficacy of the combined treatment. We introduce a specific concept of synergy between the vaccine and the PD-1 inhibitor, which is somewhat different from the usual definition of synergy. Roughly speaking, we compare the reduction in tumor size achieved by a combined therapy with amounts γ_G of GVAX and γ_A of PD-1 inhibitor to the reduction obtained by single-agent with either $(1 + \theta_G)\gamma_G$ or $(1 + \theta_A)\gamma_A$ with appropriately chosen $0 < \theta_G \leq 1$ or $0 < \theta_A \leq 1$. The larger the reduction in tumor size achieved by the combination therapy the larger the synergy is said to be. A specific choice of θ_G and θ_A, which takes into account potential negative side-effects of each drug, will be given as an example. We develop a synergy map in the (γ_G, γ_A)-plane. The map shows that, given γ_G, the synergy increases as γ_A increases as long as γ_A remains below a critical value γ_{AG}; thereafter, the synergy decreases as γ_A increases.

A discrete-time mathematical model of the combination of radiotherapy with checkpoint inhibitors was developed in [28]. Mathematical models of immunotherapy with a cancer vaccine by a system of ordinary differential equations were developed earlier in [29, 30]; these models do not consider checkpoint inhibitors. In [29] it is shown that there is a positive correlation between the number of antigen presenting cells and prolonged cancer dormancy, and in [30] it is illustrated how the combined therapy can eliminate the cancer, though neither immunotherapy nor checkpoint inhibitors can do it alone. In this paper, we present for the first time

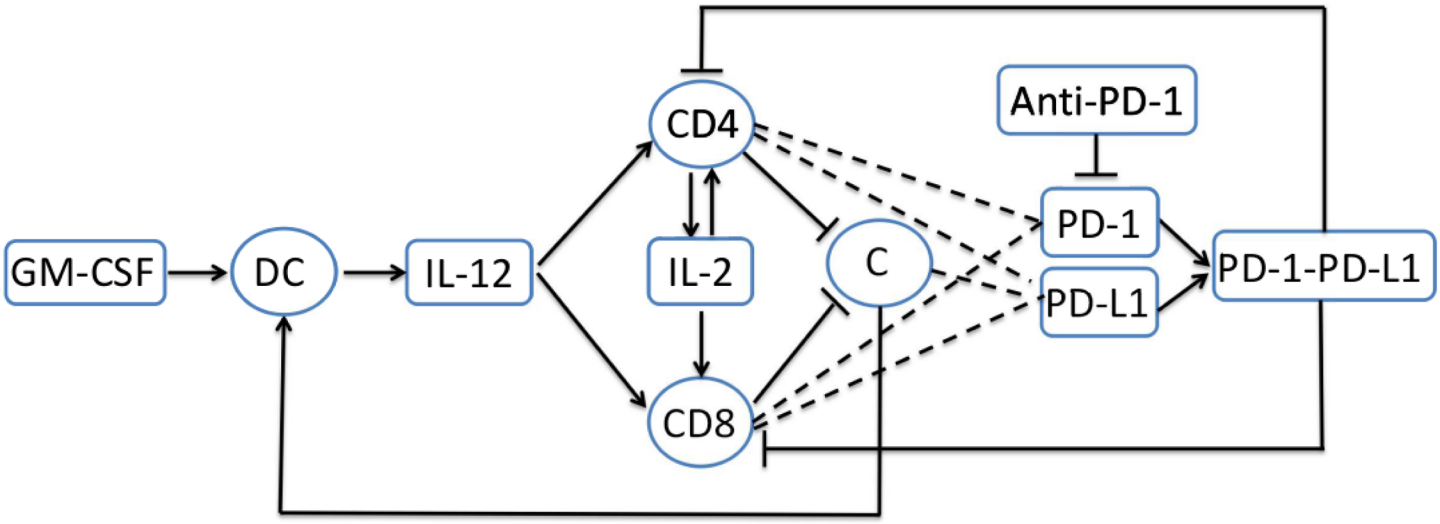

Fig 1. Interaction of immune cells with tumor cells. Sharp arrows indicate proliferation/activation, blocked arrows indicate killing/blocking, and dashed lines indicate proteins on T cells. GM-CSF activates dendritic cells; activated dendritic cells produce IL-12; IL-12 activates naive $CD4^+$ and $CD8^+$ T cells; activated $CD4^+$ T cells (Th1) produce IL-2 which induces proliferation of activated $CD4^+$ and $CD8^+$ T cells. Activated $CD4^+$ and $CD8^+$ T cells kill cancer cells. Activated $CD4^+$ and $CD8^+$ T cells express PD-1 and PD-L1, and cancer cells express PD-L1. The complex PD-1-PD-L1 inhibits the function of active $CD4^+$ and $CD8^+$ T cells.

https://doi.org/10.1371/journal.pone.0178479.g001

a mathematical model which combines a cancer vaccine with a checkpoint inhibitor: the vaccine (GVAX) increases the pool of T cells and the checkpoint inhibitor (anti-PD-1) enables the T cells to remain fully active in killing cancer cells.

Mathematical model

The mathematical model is based on the network shown in Fig 1. The list of variables, with units, is given in Table 1.

Table 1. List of variables.

Notation	Description	units
D	density of DCs	g/cm^3
T_1	density of activated $CD4^+$ T cells	g/cm^3
T_8	density of activated $CD8^+$ T cells	g/cm^3
C	density of cancer cells	g/cm^3
N_C	density of necrotic cancer cells	g/cm^3
H	HMGB-1 concentration	g/cm^3
G	GM-CSF concentration	g/cm^3
I_{12}	IL-12 concentration	g/cm^3
I_2	IL-2 concentration	g/cm^3
P	PD-1 concentration	g/cm^3
L	PD-L1 concentration	g/cm^3
Q	PD-1-PD-L1 concentration	g/cm^3
A	anti-PD-1 concentration	g/cm^3

https://doi.org/10.1371/journal.pone.0178479.t001

We assume that the total density of cancer cells (C), active dendritic cells (D), $CD4^+$ T cells (T_1) and $CD8^+$ T cells (T_8) within the tumor remains constant in space and time:

$$C + D + T_1 + T_8 = \text{ constant}. \tag{1}$$

It is tacitly assumed that the debris of dead cells, including cancer cells undergoing necrosis or apoptosis, is quickly cleared from the tumor tissue. It is also tacitly assumed that the densities of immature dendritic cells and naive $CD4^+$ and $CD8^+$ T cells are constant throughout the tumor tissue.

Under the assumption Eq (1), cancer cell proliferation, and migration of immune cells into the tumor give rise to internal pressure which results in cell movement, and we assume that all the cells move with the same velocity, **u**; **u** depends on space and time. We also assume that all the cells undergo diffusion, and that all the cytokines and drugs are diffusing within the tumor.

Equation for DCs (D). When cancer cells undergo necrosis, they release HMGB-1 [1]. We can model the dynamics of the necrotic cells and of HMGB-1 by the following equations:

$$\frac{\partial N_C}{\partial t} + \underbrace{\nabla \cdot (\mathbf{u} N_C)}_{\text{velocity}} - \underbrace{\delta_{N_C} \nabla^2 N_C}_{\text{difusion}} = \underbrace{\lambda_{N_C C} C}_{\text{derived from life cancer cells}} - \underbrace{d_{N_C} N_C}_{\text{removal}},$$

$$\frac{\partial H}{\partial t} - \underbrace{\delta_H \nabla^2 H}_{\text{difusion}} = \underbrace{\lambda_{HN_C} N_C}_{\text{released from nerotic cancer cells}} - \underbrace{d_H H}_{\text{degradation}},$$

where $\lambda_{N_C C}$ is the rate at which cancer cells become necrotic and λ_{HN_C} is the rate at which necrotic cells produce HMGB-1. We note that although molecules like HMGB-1, or other proteins, may be affected by the velocity **u**, their diffusion coefficients are several orders of magnitude larger than the diffusion coefficients of cells; hence their velocity terms may be neglected. The degradation of HMGB-1 is fast (~ 0.01/day) [31], and we assume that the removal of N_C is also fast. We can therefore approximate the two dynamical equations by the steady state equations $\lambda_{N_C C} C - d_{N_C} N_C = 0$ and $\lambda_{HN_C} N_C - d_H H = 0$, so that H is proportional to C, i.e., $H =$ constant $\times\, C$.

Dendritic cells are activated by HMGB-1 [2, 3]. Hence, the activation rate of immature dendritic cell D_0 is proportional to $D_0 \frac{C}{K_C + C}$, where the Michaelis-Menten law is used to account for the limited rate of receptor recycling time which occurs in the process of DCs activation. In the same way, GM-CSF, produced by the cancer vaccine, activates DCs at rate proportional to $D_0 \frac{G}{K_G + G}$. Hence, the dynamics of DCs is given by

$$\frac{\partial D}{\partial t} + \underbrace{\nabla \cdot (\mathbf{u} D)}_{\text{velocity}} - \underbrace{\delta_D \nabla^2 D}_{\text{difusion}} = \underbrace{\lambda_{DC} D_0 \frac{C}{K_C + C}}_{\text{activation by HMGB}-1} + \underbrace{\lambda_{DG} D_0 \frac{G}{K_G + G}}_{\text{promotion by GM}-\text{CSF}} - \underbrace{d_D D}_{\text{death}}, \tag{2}$$

where δ_D is the diffusion coefficient and d_D is the death rate of DCs.

Equation for $CD4^+$ T cells (T_1). Naive $CD4^+$ T cells are activated by IL-12, and IL-2 induces proliferation of activated T_1 cells [4, 5]. Both processes are assumed to be inhibited by the complex PD-1-PD-L1 (Q) [14], which reduces the production of T_1 cells by a factor $\frac{1}{1 + Q/K_{TQ}}$.

Hence T_1 satisfies the following equation:

$$\begin{aligned}\frac{\partial T_1}{\partial t}+\nabla\cdot(\mathbf{u}T_1)-\delta_T\nabla^2T_1 &= \underbrace{\left(\lambda_{T_1I_{12}}T_{10}\frac{I_{12}}{K_{I_{12}}+I_{12}}+\lambda_{T_1I_2}T_1\frac{I_2}{K_{I_2}+I_2}\right)}_{\text{activation by IL-12}\quad\text{IL-2-induced proliferation}}\\ &\times\underbrace{\frac{1}{1+Q/K_{TQ}}}_{\text{inhibition by PD-1-PD-L1}}-\underbrace{d_{T_1}T_1}_{\text{death}},\end{aligned}\tag{3}$$

where T_{10} is the density of naive $CD4^+$ T cells.

Equation for activated $CD8^+$ T cells (T_8). IL-12 activates $CD8^+$ T cells and IL-2 induces the proliferation of $CD8^+$ T cells [4, 5]. Hence, similarly to the equation for T_1, T_8 satisfies the equation

$$\begin{aligned}\frac{\partial T_8}{\partial t}+\nabla\cdot(\mathbf{u}T_8)-\delta_T\nabla^2T_8 &= \underbrace{\left(\lambda_{T_8I_{12}}T_{80}\frac{I_{12}}{K_{I_{12}}+I_{12}}+\lambda_{T_8I_2}T_8\frac{I_2}{K_{I_2}+I_2}\right)}_{\text{activation by IL-12}\quad\text{IL-2-induced proliferation}}\\ &\times\underbrace{\frac{1}{1+Q/K_{TQ}}}_{\text{inhibition by PD-1-PD-L1}}-\underbrace{d_{T_8}T_8}_{\text{death}},\end{aligned}\tag{4}$$

where T_{80} is the density of naive $CD8^+$ T cells.

Equation for tumor cells (C). Cancer cells are killed by T_1 and T_8 [6–8]. We assume a logistic growth with carrying capacity (C_M) in order to account for competition for space among the cancer cells. Hence,

$$\frac{\partial C}{\partial t}+\nabla\cdot(\mathbf{u}C)-\delta_C\nabla^2C = \underbrace{\lambda_CC\left(1-\frac{C}{C_M}\right)}_{\text{proliferation}}-\underbrace{(\eta_1T_1C+\eta_8T_8C)}_{\text{killing by T cells}}-\underbrace{d_CC}_{\text{death}},\tag{5}$$

where η_1, η_8 are the killing rates of cancer cells by T_1 and T_8, and d_C is the natural death rate of cancer cells.

Equation for GM-CSF (G). We assume that GVAX is injected intradermally every 3 days for 30 days (as in mouse experiments [21]) providing a source $\hat{G}(t)$ of GM-CSF, which we represent by

$$\hat{G}(t)=\begin{cases}\gamma_G & \text{if } t\le 30,\\ \gamma_G\times\frac{33-t}{3} & \text{if } 30<t\le 33,\\ 0 & \text{if } t>33.\end{cases}$$

where γ_G is the effective level of the drug; although the level of the drug varies between injections, for simplicity we take it to be constant. The concentration of GM-CSF in tissue is very small [32], and accordingly, we assume a low rate of constant source λ_G for GM-CSF. Hence G satisfies the following equation:

$$\frac{\partial G}{\partial t}-\delta_G\nabla^2G = \lambda_G+\hat{G}(t)-\underbrace{d_GG}_{\text{degradation}},\tag{6}$$

where d_G is the degradation rate of GM-CSF.

Equation for IL-12 (I_{12}). IL-12 is produced by activated DCs [4, 5], so that

$$\frac{\partial I_{12}}{\partial t} - \delta_{I_{12}} \nabla^2 I_{12} = \underbrace{\lambda_{I_{12}D} D}_{\text{production by DCs}} - \underbrace{d_{I_{12}} I_{12}}_{\text{degradation}}. \tag{7}$$

Equation for IL-2 (I_2). IL-2 is produced by activated CD4$^+$ T cells (T_1) [4, 5]. Hence,

$$\frac{\partial I_2}{\partial t} - \delta_{I_2} \nabla^2 I_2 = \underbrace{\lambda_{I_2 T_1} T_1}_{\text{production by } T_1} - \underbrace{d_{I_2} I_2}_{\text{degradation}}. \tag{8}$$

Equation for PD-1 (P), PD-L1 (L) and PD-1-PD-L1 (Q). PD-1 is expressed on the surface of activated CD4$^+$ T cells and activated CD8$^+$ T cells [14, 15]. We assume that the expression level of PD-1 is the same for activated CD4$^+$ and CD8$^+$ T cells. Hence, P is given by

$$P = \rho_P (T_1 + T_8),$$

where ρ_P is the ratio between the mass of one PD-1 protein to the mass of one T cell. The coefficient ρ_P is constant when no anti-PD-1 drug is injected. In that case, to a change in $T = T_1 + T_8$, given by $\frac{\partial T}{\partial t}$, there corresponds a change of P, given by $\rho_P \frac{\partial T}{\partial t}$. For the same reason, $\nabla \cdot (\mathbf{u}P) = \rho_P \nabla \cdot (\mathbf{u}T)$ and $\nabla^2 P = \rho_P \nabla^2 T$ when no anti-PD-1 drug is injected. Hence, P satisfies the equation

$$\frac{\partial P}{\partial t} + \nabla \cdot (\mathbf{u}P) - \delta_T \nabla^2 P = \rho_P \left[\frac{\partial (T_1 + T_8)}{\partial t} + \nabla \cdot (\mathbf{u}(T_1 + T_8)) - \delta_T \nabla^2 (T_1 + T_8) \right].$$

Recalling Eqs (3) and (4) for T_1 and T_8, we get

$$\begin{aligned} \frac{\partial P}{\partial t} + \nabla \cdot (\mathbf{u}P) - \delta_T \nabla^2 P = {} & \rho_P \left[(\lambda_{T_1 I_{12}} T_{10} + \lambda_{T_8 I_{12}} T_{80}) \frac{I_{12}}{K_{I_{12}} + I_{12}} \right. \\ & \left. + (\lambda_{T_1 I_2} T_1 + \lambda_{T_8 I_2} T_8) \frac{I_2}{K_{I_2} + I_2} \right] \times \frac{1}{1 + Q/K_{TQ}} \\ & - \rho_P (d_{T_1} T_1 + d_{T_8} T_8). \end{aligned}$$

When anti-PD-1 drug (A) is applied, PD-1 is depleted (or blocked) by A. In this case, the ratio $\frac{P}{T_1 + T_8}$ may change. In order to include in the model both cases of with and without anti-PD-1, we replace ρ_P in the previous equation by $\frac{P}{T_1 + T_8}$. Hence,

$$\begin{aligned} \frac{\partial P}{\partial t} + \nabla \cdot (\mathbf{u}P) - \delta_T \nabla^2 P = {} & \frac{P}{T_1 + T_8} \left[(\lambda_{T_1 I_{12}} T_{10} + \lambda_{T_8 I_{12}} T_{80}) \frac{I_{12}}{K_{I_{12}} + I_{12}} \right. \\ & \left. + (\lambda_{T_1 I_2} T_1 + \lambda_{T_8 I_2} T_8) \frac{I_2}{K_{I_2} + I_2} \right] \times \frac{1}{1 + Q/K_{TQ}} \\ & - \frac{P}{T_1 + T_8} (d_{T_1} T_1 + d_{T_8} T_8) - \underbrace{\mu_{PA} P A}_{\text{depletion by anti-PD-1}}, \end{aligned} \tag{9}$$

where μ_{PA} represents the rate at which P is depleted/blocked by A.

PD-L1 is expressed on the surface of activated CD4$^+$ and CD8$^+$ T cells [14, 15] and on cancer cells [15, 16]. Hence, the concentration of PD-L1 (L) is proportional to $(T_1 + T_8)$ and C:

$$L = \rho_L (T_1 + T_8 + \varepsilon C), \tag{10}$$

where ε depends on the specific type of tumor.

PD-L1 from T cells or cancer cells ligands to PD-1 on the plasma membrane of T cells, thus forming a complex PD-1-PD-L1 (Q) on the T cells [15, 16]. Denoting the association and dissociation rates of Q by α_{PL} and d_Q, respectively, we can write

$$P + L \underset{d_Q}{\overset{\alpha_{PL}}{\rightleftharpoons}} Q, \tag{11}$$

so that

$$\frac{\partial Q}{\partial t} + \nabla \cdot (\mathbf{u}Q) - \delta_T \nabla^2 Q = \alpha_{PL} PL - d_Q Q.$$

The half-life of Q is less then 1 second (i.e. 1.16×10^{-5} day) [33], and hence d_Q is very large, and we may approximate the dynamical equation by the steady state equation, $\alpha_{PL}PL = d_Q Q$, or

$$Q = \sigma PL, \tag{12}$$

where $\sigma = \alpha_{PL}/d_Q$.

Equation for anti-PD-1 (A). We assume that anti-PD-1 is injected intradermally every 3 days for 30 days (as in mouse experiments [21]) providing a source $\hat{A}(t)$ of anti-PD-1:

$$\hat{A}(t) = \begin{cases} \gamma_A & \text{if } t \leq 30, \\ \gamma_A \times \frac{33-t}{3} & \text{if } 30 < t \leq 33, \\ 0 & \text{if } t > 33. \end{cases}$$

where γ_A is the effective level of the drug; although the level of the drug varies between injections, for simplicity we take it to be constant. The drug A is depleted in the process of blocking PD-1. Hence,

$$\frac{\partial A}{\partial t} - \delta_A \nabla^2 A = \hat{A}(t) - \underbrace{\mu_{PA} PA}_{\text{depletion through blocking PD-1}} - \underbrace{d_A A}_{\text{degradation}}, \tag{13}$$

where μ_{PA} is the rate at which A is degraded in the process of blocking PD-1.

Equation for cell velocity (u): We assume that most of the tumor consists of the extracellular matrix, ECM (approximately, 0.6 g/cm^3), and cancer cells (approximately, $C = 0.4$ g/cm^3), and that the densities of D, T_1 and T_8 are approximately 4×10^{-4}, 2×10^{-3} and 1×10^{-3} g/cm^3, respectively (as explained in the section on parameter estimation). We further assume that all cells are approximately of the same volume and surface area, so that their diffusion coefficients are the same. For definiteness, we take the constant in Eq (1) to be 0.4034. Adding Eqs (2)–(5), we then get

$$0.4034 \times \nabla \cdot \mathbf{u} = \sum_{j=2}^{5} [\text{RHS of Eq. } (j)]. \tag{14}$$

To simplify the computations, we shall assume that the tumor is spherical and denote its moving boundary (i.e. its radius) by $r = R(t)$. We also assume that all the densities and concentrations are radially symmetric, that is, functions of (r, t), where $0 \leq r \leq R(t)$. In particular, $\mathbf{u} = u(r, t)\mathbf{e}_r$, where $\mathbf{e}_r$ is the unit radial vector, and each of the equations of the form

$$\frac{\partial X}{\partial t} + \nabla \cdot (\mathbf{u}X) - \delta_X \nabla^2 X = F,$$

with $X = X(r, t)$, takes the form

$$\frac{\partial X}{\partial t} + \frac{1}{r^2}\frac{\partial}{\partial r}(r^2 uX) - \delta_X \frac{1}{r^2}\frac{\partial}{\partial r}\left(r^2 \frac{\partial X}{\partial r}\right) = F.$$

Equation for free boundary (*R*): We assume that the free boundary $r = R(t)$ moves with the velocity of cells, so that

$$\frac{dR(t)}{dt} = u(R(t), t). \tag{15}$$

Boundary conditions We assume that the naive $CD4^+$ T cells and naive $CD8^+$ T cells which migrated from the lymph nodes into the tumor microenvironment have constant densities $\hat{T}_1$ and $\hat{T}_8$ at the tumor boundary, and that they are activated by IL-12 upon entering the tumor. We represent this process by the flux conditions at the boundary $r = R(t)$:

$$\frac{\partial T_1}{\partial r} + \sigma_T(I_{12})(T_1 - \hat{T}_1) = 0, \ \frac{\partial T_8}{\partial r} + \sigma_T(I_{12})(T_8 - \hat{T}_8) = 0, \tag{16}$$

where $\sigma_T(I_{12}) = \sigma_0 \frac{I_{12}}{I_{12}+K_{I_{12}}}$.

We impose the no-flux boundary conditions for all the remaining variables:

$$\begin{aligned} \text{No} - \text{flux for } & D(r,t), C(r,t), G(r,t), I_{12}(r,t), I_2(r,t), \\ & P(r,t) \text{ and } A(r,t), \quad \text{at } r = R(t). \end{aligned} \tag{17}$$

It is tacitly assumed here that the receptors PD-1 and ligands PD-L1 become active only after the T cells are inside the tumor.

Initial conditions. We take initial values of all the variables to be constant. Later on we shall compare the simulations of the model with mouse experimental results, for 60 days. Accordingly, we take initial values whereby the average density of cancer cells has not yet increased to its steady state, 0.4 g/cm^3, and, in view of Eq (1), the total density of the immune cells is initially above its steady state. We take (in unit of g/cm^3):

$$D = 6 \times 10^{-4}, \ T_1 = 4 \times 10^{-3}, \ T_8 = 2 \times 10^{-3}, \ C = 0.3968. \tag{18}$$

We assume that initially $A = 0$, and

$$\begin{aligned} G &= 2.61 \times 10^{-10} \text{ g/ cm}^3, \ I_{12} = 1.8 \times 10^{-10} \text{ g/ cm}^3, \ I_2 = 4.74 \times 10^{-11} \text{ g/ cm}^3, \\ P &= 11.2 \times 10^{-10} \text{ g/ cm}^3. \end{aligned}$$

These values are close to the steady state values which are computed in the section on parameter estimation.

Results

The simulations of the model were performed by Matlab based on the moving mesh method for solving partial differential equations with free boundary [34] (see the section on computational method). All the computations are done in dimensionless form, but displayed in dimensional form.

The average density or concentration of a species is defined as its total mass in the tumor divided by the tumor volume. Fig 2 shows the average concentrations of all the species of the model over a period of 60 days in the control case, that is, when no drugs are administered; the parameter values are given in Tables 2 and 3. The radius of the tumor is increasing, from 0.01

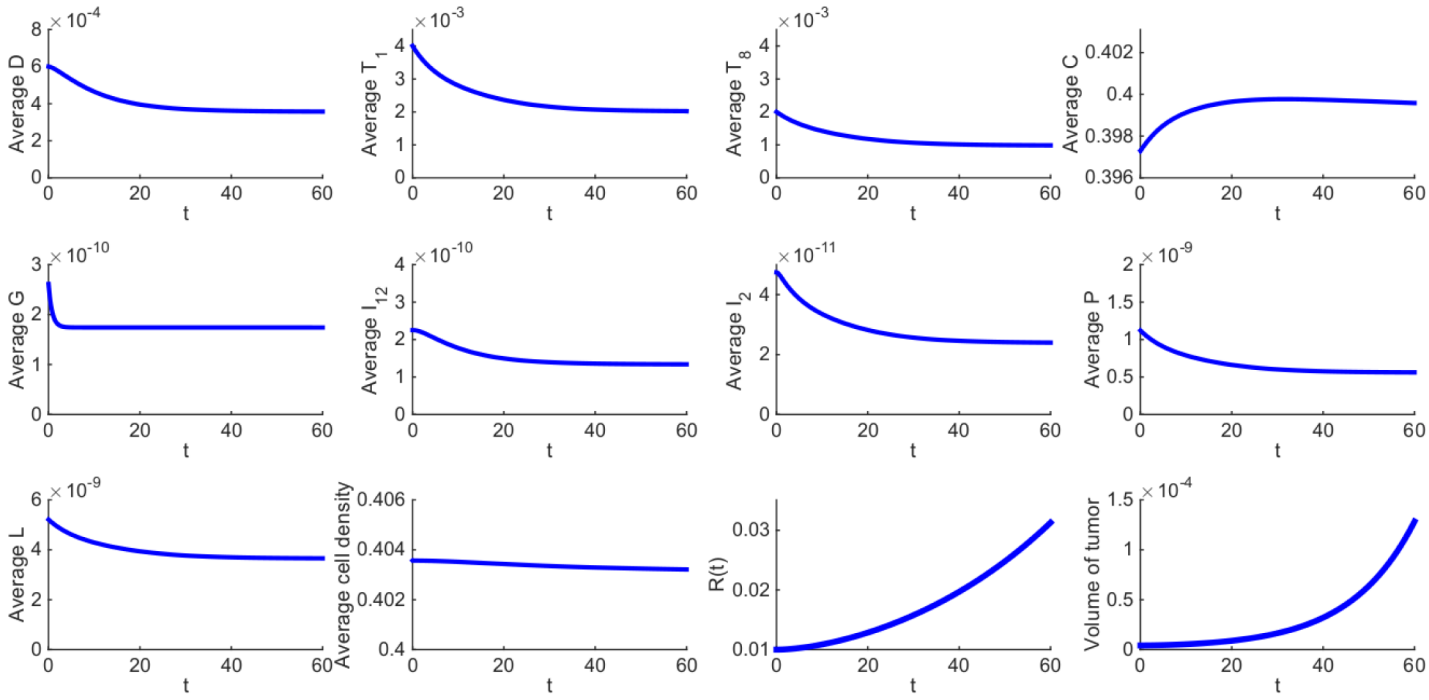

Fig 2. Average densities/concentrations of all the variables in the model in the control case (no drugs). Figures in the first and second panels and the first figure in the third panel show the average density or concentration of each species in the model. The last three figures in the third panel show the total average density of all cells, the growth of tumor radius and the growth of tumor volume, respectively. All parameter values are the same as in Tables 2 and 3.

https://doi.org/10.1371/journal.pone.0178479.g002

cm to 0.0313 cm. The average density of the cancer cells is initially increasing and later it stabilizes while the densities of the immune cells are first decreasing and later stabilize. Correspondingly, the concentrations of the cytokines produced by the immune system also first decrease and later stabilize. Some of the parameters in the model were estimated by assuming the immune cells and cytokines are in steady state. Their steady states in Fig 2 approximately agree with those which we assumed in estimating the parameters, thus establishing the consistency of our assumed steady-state values.

We can also simulate the spatial distribution of each of the variables. Fig 3 shows the distribution of cancer cells and T cells ($T_1 + T_8$) at times $t = 15, 30, 60$ days. We see that the density of T cells increases toward the boundary; this is a result of the influx of T cells from the lymph nodes. Correspondingly, the density of cancer cells decreases toward the boundary. In our model, we tacitly assumed avascular conditions, since we wanted to focus primarily on the difference between control and treatment. Since, however, the tumor radius reaches approximately 313 μm at day 60, hypoxic conditions may actually reduce the cancer cells' density at the core of the tumor (both in control and treatment).

In Figs 2 and 3, we have taken $\varepsilon = 0.01$. Some cancer cells may express more or less PD-L1 [17, 35–37]. By decreasing or increasing ε, the radius of the tumor will decrease or increase, respectively, but the profiles of the densities/concentrations remain qualitatively the same (not shown here).

We next proceed to explore the effect of treatment with GM-CSF-secreting vaccine (GVAX) and anti-PD-1 drug. We are unable to make a direct connection between the levels of

Table 2. Summary of parameter values.

Notation	Description	Value used	References
δ_D	diffusion coefficient of DCs	8.64×10^{-7} cm^2 day^{-1}	[59]
δ_{T_1}	diffusion coefficient of CD4$^+$ T cells	8.64×10^{-7} cm^2 day^{-1}	[59]
δ_{T_8}	diffusion coefficient of CD8$^+$ T cells	8.64×10^{-7} cm^2 day^{-1}	[59]
δ_C	diffusion coefficient of tumor cells	8.64×10^{-7} cm^2 day^{-1}	[59]
δ_G	diffusion coefficient of GM-CSF	9.8495×10^{-2} cm^2 day^{-1}	estimated
$\delta_{I_{12}}$	diffusion coefficient of IL-12	6.0472×10^{-2} cm^2 day^{-1}	estimated
δ_{I_2}	diffusion coefficient of IL-2	9.9956×10^{-2} cm^2 day^{-1}	estimated
δ_A	diffusion coefficient of anti-PD-1	7.85×10^{-2} cm^2 day^{-1}	estimated
σ_0	flux rate of T cells on the boundary	1 cm^{-1}	[59]
λ_{DG}	activation rate of DCs by GM-CSF	20.02 day^{-1}	[65, 66] & estimated
λ_{DC}	activation rate of DCs by tumor cells	0.364 day^{-1}	estimated
$\lambda_{T_1I_{12}}$	activation rate of CD4$^+$ T cells by IL-12	4.66 day^{-1}	estimated
$\lambda_{T_1I_2}$	activation rate of CD4$^+$ T cells by IL-2	0.25 day^{-1}	estimated
$\lambda_{T_8I_{12}}$	activation rate of CD8$^+$ T cells by IL-12	4.15 day^{-1}	estimated
$\lambda_{T_8I_2}$	activation rate of CD8$^+$ T cells by IL-2	0.25 day^{-1}	[59]
λ_C	growth rate of cancer cells	0.616 day^{-1}	[59]
λ_G	non-vaccine source of GM-CSF	2.23×10^{-10} g/cm^3 · day	estimated
$\lambda_{I_{12}D}$	production rate of IL-12 by DCs	5.18×10^{-7} day^{-1}	estimated
$\lambda_{I_2T_1}$	production rate of IL-2 by CD4$^+$ T cells	2.82×10^{-8} day^{-1}	estimated
η_1	killing rate of tumor cells by CD4$^+$ T cells	11.5 day^{-1} · cm^3/g	estmated
η_8	killing rate of tumor cells by CD8$^+$ T cells	46 day^{-1} · cm^3/g	estimated
μ_{PA}	blocking rate of PD-1 by anti-PD-1	6.87×10^6 cm^3/g · day	estimated
ρ_P	expression of PD-1 in T cells	2.49×10^{-7}	estimated
ρ_L	expression of PD-L1 in T cells	5.22×10^{-7}	estimated
ε	expression of PD-L1 in tumor cells	0 − 0.01*	estimated
d_D	death rate of DCs	0.1 day^{-1}	[59]
d_{T_1}	death rate of CD4$^+$ T cells	0.197 day^{-1}	[59]
d_{T_8}	death rate of CD8$^+$ T cells	0.18 day^{-1}	[59]
d_C	death rate of tumor cells	0.17 day^{-1}	[59]
d_G	degradation rate of GM-CSF	1.28 day^{-1}	[65]
$d_{I_{12}}$	degradation rate of IL-12	1.38 day^{-1}	[59]
d_{I_2}	degradation rate of IL-2	2.376 day^{-1}	[59]
d_A	degradation rate of anti-PD-1	0.0462 day^{-1}	[42]

* In the simulations we took $\varepsilon = 0.01$.

https://doi.org/10.1371/journal.pone.0178479.t002

drugs administered to the patient, and their 'effective strengths' γ_G and γ_A in the model, since these data are not available. Based on the estimate of the concentration of GM-CSF in normal healthy tissue (see Parameter Estimations for Eq (6)), we chose the order of magnitude of GVAX to be 10^{-10} (g/cm^3 · day). The order of magnitude for anti-PD-1 drug (γ_A) is chosen so as to get the best agreement with the mouse experiments. In Fig 4(a), the 'effective strength' of the vaccine is given by $\gamma_G = 0.87 \times 10^{-10}$ g/cm^3 · day and the 'effective strength' of the anti-PD-1 is given by $\gamma_A = 2 \times 10^{-10}$ g/cm^3 · day. We see that, as a single-agent, anti-PD-1 is more effective than GVAX, and with the combined therapy the tumor radius is still increasing. This is in agreement with the mouse experiments reported in Fig 1-(A) (with melanoma) in [21], and Figs 3-(b) (with colon carcinoma) and 3-(c) (with melanoma) in [22].

Table 3. Summary of parameter values.

K_G	half-saturation of GM-CSF	1.74×10^{-9} g/cm^3	[65]
K_C	half-saturation of tumor cells	0.4 g/cm^3	[59]
$K_{I_{12}}$	half-saturation of IL-12	1.5×10^{-10} g/cm^3	[59]
K_{I_2}	half-saturation of IL-2	2.37×10^{-11} g/cm^3	[59]
K_{T_1}	half-saturation of CD4$^+$ T cells	2×10^{-3} g/cm^3	estimated
K_{T_8}	half-saturation of CD8$^+$ T cells	1×10^{-3} g/cm^3	estimated
K'_{TQ}	inhibition of function of T cells by PD-1-PD-L1	1.365×10^{-18} g/cm^3	estimated
D_0	density of immature DCs	2×10^{-5} g/cm^3	[59]
T_{10}	density of naive CD4$^+$ T cells	4×10^{-4} g/cm^3	estimated
T_{80}	density of naive CD8$^+$ T cells	2×10^{-4} g/cm^3	estimated
C_M	carrying capacity of cancer cells	0.8 g/cm^3	[59]
$\hat{T}_1$	density of CD4$^+$ T cells from lymph node	4×10^{-3} g/cm^3	estimated
$\hat{T}_8$	density of CD8$^+$ T cells from lymph node	2×10^{-3} g/cm^3	estimated
γ_G	source of GM-CSF from the vaccine	1×10^{-10} g/cm^3 · day*	estimated
γ_A	source of anti-PD-1	1×10^{-10} g/cm^3 · day*	estimated

* Values used in sensitivity analysis.

https://doi.org/10.1371/journal.pone.0178479.t003

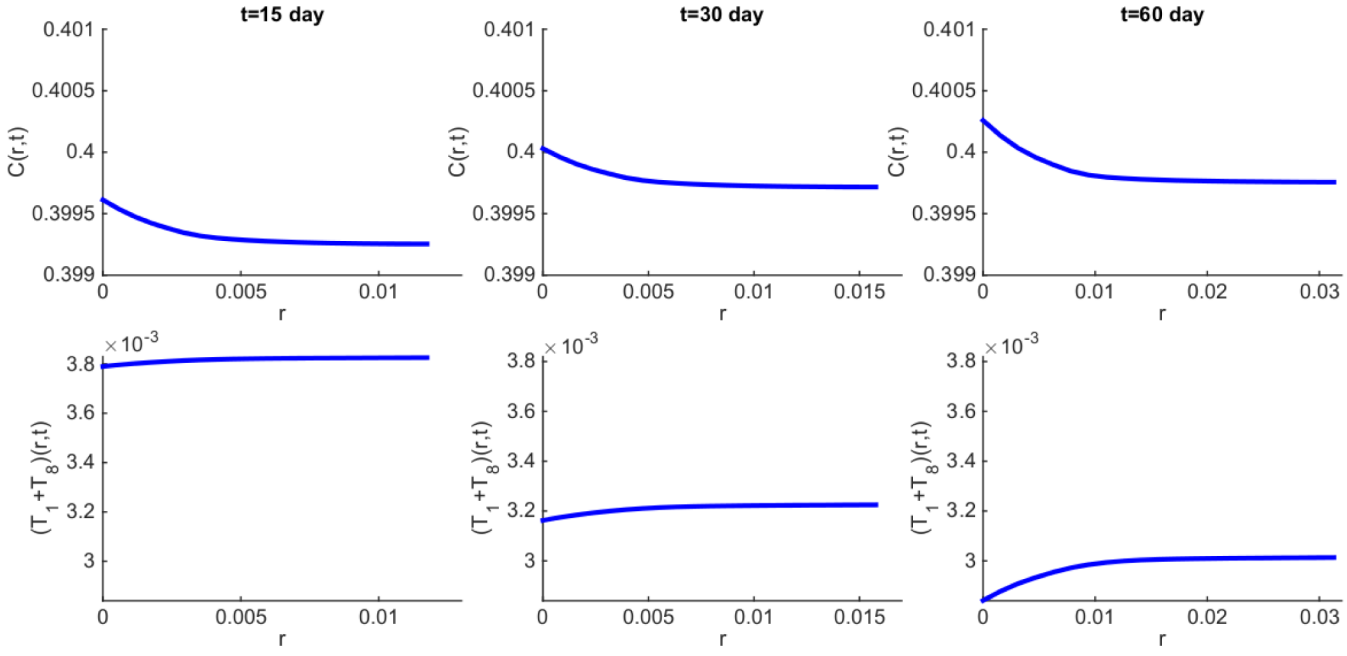

Fig 3. Spatial distribution of density of cancer cells and T_1 + T_8 cells at time t = 15, 30, 60 days. All parameter values are the same as in Fig 2.

https://doi.org/10.1371/journal.pone.0178479.g003

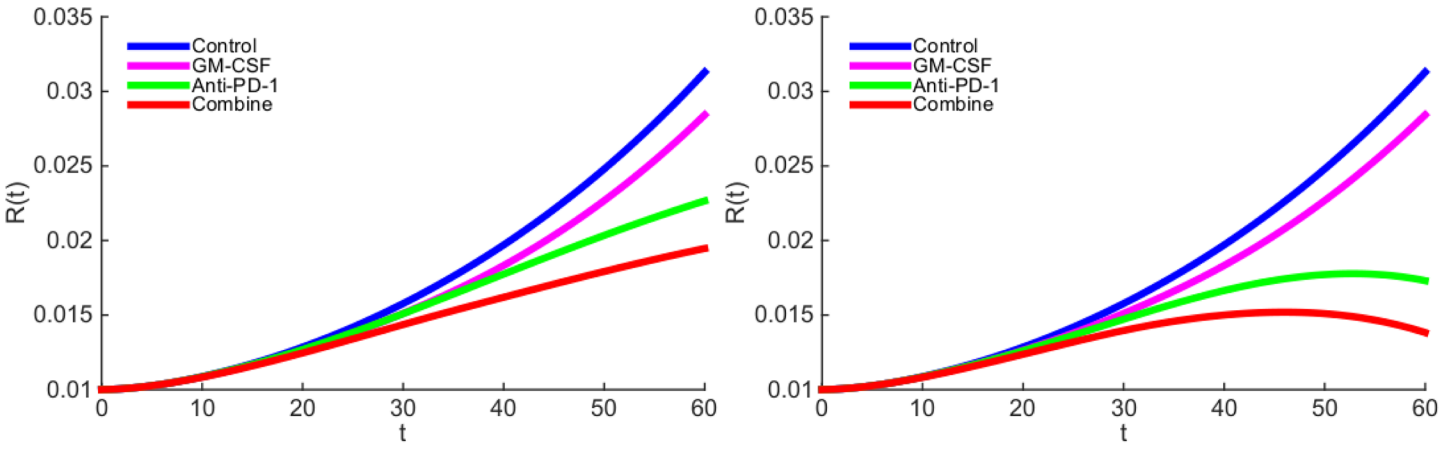

Fig 4. The growth of tumor radius $R(t)$ during the administration of GM-CSF-secreting vaccine and anti-PD-1 drug. (a) GM-CSF-secreting vaccine is administered at rate $\gamma_G = 0.87 \times 10^{-10}$ g/cm^3 · day and anti-PD-1 drug is administered at rate $\gamma_A = 2 \times 10^{-10}$ g/cm^3 · day. (b) GM-CSF-secreting vaccine is administered at rate $\gamma_G = 0.87 \times 10^{-10}$ g/cm^3 · day and anti-PD-1 drug is administered at rate $\gamma_A = 3 \times 10^{-10}$ g/cm^3 · day.

https://doi.org/10.1371/journal.pone.0178479.g004

In Fig 4(b), we increased γ_A by a factor 3/2. As a result, the tumor radius begins to decrease around day 50, even when administering anti-PD-1 as single-agent. This is in agreement with mouse experiments (with colon carcinoma) reported in Fig 1-(D) of [23].

In Fig 4(a), GM-CSF-secreting vaccine alone did not reduce the tumor radius as much as anti-PD-1 alone. However, if we increase the strength of the vaccine and decrease the anti-PD-1, taking for example, $\gamma_G = 3.84 \times 10^{-10}$ g/cm^3 · day and $\gamma_A = 1 \times 10^{-10}$ g/cm^3 · day, we then find that the vaccine decreases the tumor radius more than anti-PD-1 does; this is shown in Fig 5, and it is in agreement with mouse experiments (with melanoma) reported in Fig 1-(B) of [23].

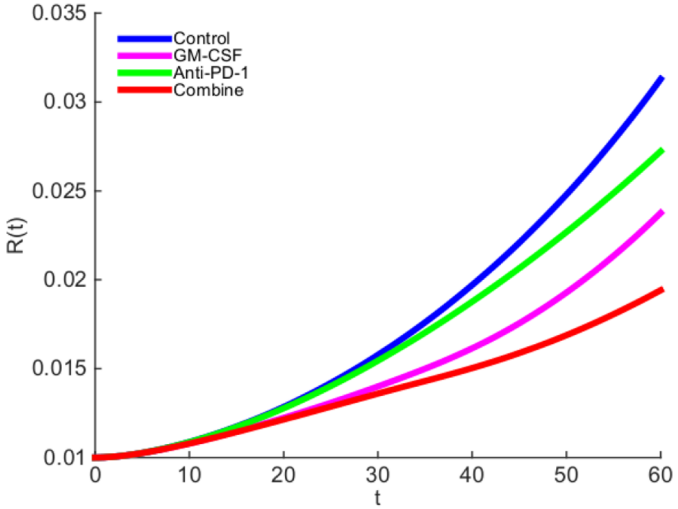

Fig 5. The growth of tumor radius $R(t)$ during the administration of GM-CSF-secreting vaccine and anti-PD-1 drug. GM-CSF-secreting vaccine is administered at rate $\gamma_G = 3.84 \times 10^{-10}$ g/cm^3 · day and anti-PD-1 drug is administered at rate $\gamma_A = 1 \times 10^{-10}$ g/cm^3 · day.

https://doi.org/10.1371/journal.pone.0178479.g005

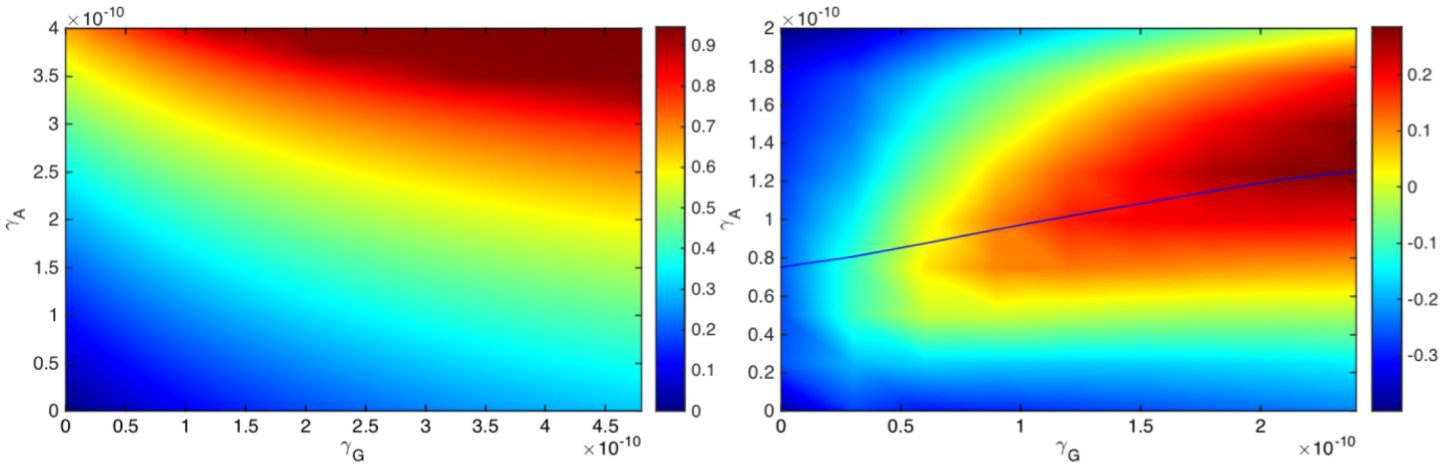

Fig 6. Drug efficacy map and synergy map. (a) Efficacy map: The color column shows the efficacy $E(\gamma_G, \gamma_A)$ when γ_G varies between $0 - 4.8 \times 10^{-10}$ g/cm^3 · day and γ_A varies between $0 - 4 \times 10^{-10}$ g/cm^3 · day. (b) Synergy map: The color column shows the synergy $\sigma(\gamma_G, \gamma_A)$ when γ_G varies between $0 - 2.4 \times 10^{-10}$ g/cm^3 · day and γ_A varies between $0 - 2 \times 10^{-10}$ g/cm^3 · day. For a given γ_G, the optimal synergy of the combined therapy (γ_G, γ_A) occurs when (γ_G, γ_A) lies on the solid curve.

https://doi.org/10.1371/journal.pone.0178479.g006

The results of Figs 4 and 5 show that a combination therapy of GVAX and anti-PD-1 in appropriate amounts could significantly slow the growth of a tumor.

There is some uncertainty in the estimates of some of the parameters of the model. With somewhat different choices of these parameters, the simulation results will change quantitatively, and sensitivity analysis indicates the direction and intensity of the change (see the section on sensitivity analysis). In particular, the choice of γ_G and γ_A will affect the relative reduction in the growth of the tumor radius. In Figs 4 and 5 we made specific choices of γ_G and γ_A, in order to get simulations that agree with experimental results.

We next consider combination therapy for any values of GVAX and anti-PD-1. We define the efficacy of the combination therapy with (γ_G, γ_A) by the formula:

$$E(\gamma_G, \gamma_A) = \frac{R_{60}(0,0) - R_{60}(\gamma_G, \gamma_A)}{R_{60}(0,0)},$$

where $R_{60} = R_{60}(\gamma_G, \gamma_A)$ represents the tumor radius computed at day 60. If the tumor radius at day 60, $R_{60}(\gamma_G, \gamma_A)$, is smaller than the radius in the control case, $R_{60}(0, 0)$, then the efficacy is a positive number, and its value is between 0 and 1 (or between 0% and 100%); the efficacy increases to 1 (or to 100%) when the tumor radius $R_{60}(\gamma_G, \gamma_A)$ decreases to 0 by day 60. Fig 6 (a) is the efficacy map of the combined therapy with γ_G in the range of $0 - 4.8 \times 10^{-10}$) g/cm^3 · day and γ_A in the range of $0 - 4 \times 10^{-10}$ g/cm^3 · day. The color column in Fig 6(a) shows the efficacy for any pair of (γ_G, γ_A); the efficacy is positive, and its maximum is 0.95 (95%). We see that an increase in either γ_G or γ_A improves the efficacy of the treatment.

Early stage clinical trials consider the safety of each of the drugs, GVAX and anti-PD-1, separately. In the GVAX treatment of patients with pancreatic cancer, no dose-limiting toxicity or minimal toxicity was observed [38–40]. On the other hand, in treatment with anti-PD-1, mild to moderate toxicity (grades 1 and 2) was observed in melanoma [41, 42]. In non-small-cell lung cancer, 14% of the patients were observed to have more severe toxicity (grades 3 and 4) [43]. Based on these observations we conclude that anti-PD-1 causes more toxicity than

GVAX. However, clinical trials on the safety and efficacy of the combined drugs are limited [23, 44, 45].

The amount of drug in clinical trials is constrained by the maximum tolerated dose (MTD). In combination therapy this constraint may depend on the proportion between the amounts of the drugs. We note that there is a large literature on the trade-off between efficacy and toxicity [46–49]. Here we consider, as an example, two treatments, (γ_G^*, γ_A^*) and $(\gamma_G^{**}, \gamma_A^{**})$, with $\gamma_G^* > \gamma_G^{**}$ and $\gamma_A^* < \gamma_A^{**}$, where both satisfy the MTD requirement. The question is then which of the two treatments is more effective in reducing the tumor volume. We can use the efficacy map to address such a question. We illustrate this in one special case.

We compare treatment of combination (γ_G, γ_A) with monotherapy GVAX and monotherapy anti-PD-1. For monotherapy with GVAX, we take $(1 + \theta_G)\gamma_G$, and for monotherapy with anti-PD-1 we take $(1 + \theta_A)\gamma_A$, with $\theta_A < \theta_G$, to reflect the higher toxicity associated with anti-PD-1. If $E(\gamma_G, \gamma_A)$ is larger than both $E((1 + \theta_G)\gamma_G, 0)$ and $E(0, (1 + \theta_A)\gamma_A)$, then we say that the synergy for the combination (γ_G, γ_A) is positive, and otherwise, we say that the synergy is negative. More generally, we define the synergy $\sigma = \sigma(\gamma_G, \gamma_A)$ by the formula:

$$\sigma(\gamma_G, \gamma_A) = \frac{E(\gamma_G, \gamma_A)}{\max\{E((1 + \theta_G)\gamma_G, 0), E(0, (1 + \theta_A)\gamma_A)\}} - 1. \tag{19}$$

Thus $\sigma(\gamma_G, \gamma_A) > 0$ (positive synergy) if the combination (γ_G, γ_A) reduces tumor growth more than either one of the single agents with $(1 + \theta_G)\gamma_G$ or $(1 + \theta_A)\gamma_A$. Negative synergy occurs in the reverse case where instead of a combination therapy with (γ_G, γ_A) we achieve better reduction of the tumor radius R_{60} if we apply only one drug, $(1 + \theta_G)\gamma_G$ or $(1 + \theta_A)\gamma_A$. The above concept of synergy is somewhat different from the usual definitions of synergy. For definiteness we take $\theta_G = 1$ and $\gamma_A = 0.5$, but this choice, which is somewhat arbitrary, could be made more precise as more clinical data become available.

Fig 6(b) is the synergy map for (γ_G, γ_A) in the same range as in Fig 6(a); the color column shows the synergy $\sigma(\gamma_G, \gamma_A)$, with values that vary from -0.38 to 0.28.

We first note that the synergy is negative if $\gamma_G < 0.2 \times 10^{-10}$ g/cm^3 · day. The reason is the following: if γ_G is small then the numbers of T cells is also small, so instead of introducing a drug γ_A which blocks the relatively small number of PD-1, it is more effective to increase the number of T cells by increasing γ_G, i.e. $E(2\gamma_G, 0) > E(\gamma_G, \gamma_A)$.

Next, for any fixed γ_G, as seen in Fig 6(b), the synergy first increases with γ_A and then decreases. In order to explain this occurrence, we note that with γ_G fixed, the number of T cells that arrive into the tumor microenvironment is limited, and so is the number of their PD-1. Thus, in order to block the PD-1 there is a need for only a limited amount of anti-PD-1 drug; i.e. it is 'wasteful' to administer too much of γ_A. We conclude that the maximum synergy is achieved when the amount of γ_A is appropriately dependent on the amount of γ_G, as indicated by the solid curve shown in Fig 6(b).

Fig 7 shows that as the amounts of γ_G and γ_A increase the average density of T cells ($T_1 + T_8$) increases, and correspondingly the average density of cancer cells decreases. We also see that the density of T cells shown in the color column increases approximately by a factor of 6, whereas the density of cancer cells decreases approximately by a factor of 1.075. The proportion of these changes (i.e. 5/0.075) is similar to the proportion of densities of cancer cells to T cells.

Conclusion

The introduction of immune checkpoint inhibitors has been a very promising approach to cancer treatment. Blockage of the programmed death PD-1/PD-L1 is increasingly explored in

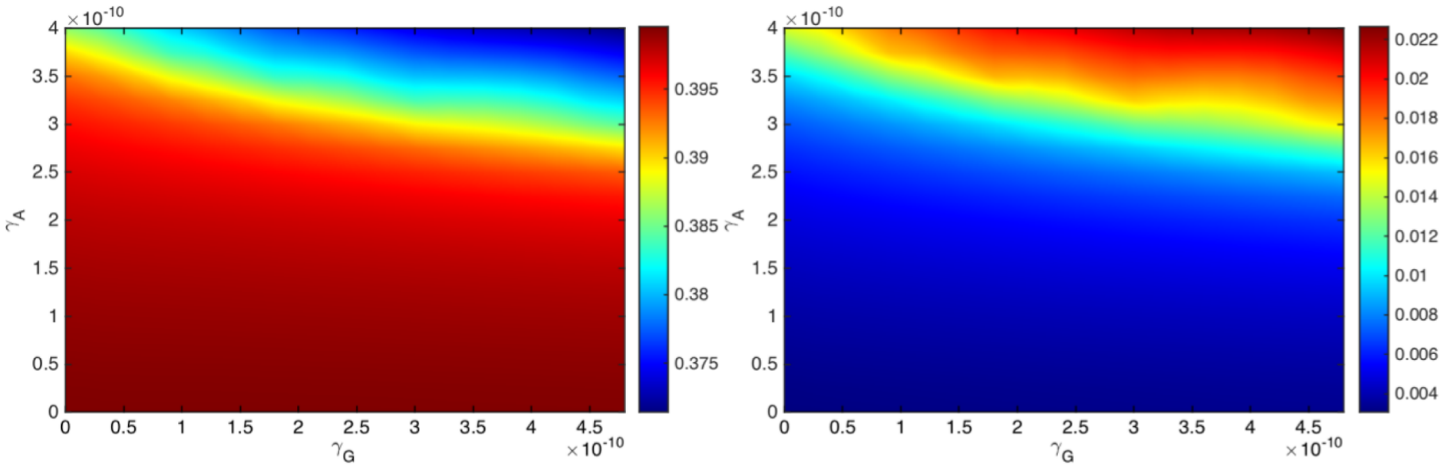

Fig 7. Average densities of cancer cells and T cells. (a) The average density of cancer cells (C), and (b) the average density of T cells ($T_1 + T_8$), under the combination of the drugs with (γ_G, γ_A), where γ_G varies between $0 - 4.8 \times 10^{-10}$ g/cm^3 · day and γ_A varies between $0 - 4 \times 10^{-10}$ g/cm^3 · day.

https://doi.org/10.1371/journal.pone.0178479.g007

single-agent studies [16, 18]. However, because of the lack of tumor-infiltrating effector T cells, many patients do not respond to checkpoint inhibitor treatment as single-agent [18]. On the other hand, cancer vaccines have been shown to induce effector T-cells infiltration into tumors [19], although, to be fully effective, cancer vaccines have to overcome immune evasion [10]. It was recently suggested that the combination of a cancer vaccine and an immune checkpoint inhibitor may function synergistically to induce more effective antitumor immune response [18, 20]. Clinical trials to test such combinations are currently ongoing [18, 20].

In the present paper we developed a mathematical model to study the efficacy of the combination of a GM-CSF-secreting cancer vaccine (GVAX) and an anti-PD-1 drug, and to address the following question: at what proportion should the two drugs be administered in order to achieve the best efficacy when the amount of drugs is limited by MTD. The mathematical model is represented by a system of partial differential equations, based on the interactions among cancer cells, dendritic cells, $CD4^+$ and $CD8^+$ T cells, cytokines IL-12 and IL-2, GM-CSF, PD-1, PD-L1, PD-1-PD-L1 complex and anti-PD-1. Simulations of the model are shown to be in qualitative agreement with mouse experiments [21–23].

The cancer vaccine and the anti-PD-1 work in collaboration: The vaccine increases the number of tumor-infiltrating effector T cells and the anti-PD-1 ensures that these cells remain active. Given a fixed amount γ_G of the vaccine and γ_A of the anti-PD-1, it is important to estimate the level of synergy between these amounts in order to administer them in the most effective proportion. We introduced a specific concept of synergy $\sigma(\gamma_G, \gamma_A)$ and developed accordingly a synergy map in Fig 6(b). The map shows that if γ_G is small, single-agent treatment (with $\gamma_A = 0$) is the best treatment. Fig 6(b) also shows that, for any γ_G, there is a unique value γ_{AG}, such that the synergy increases as γ_A increases as long as γ_A remains smaller than γ_{AG}, but the synergy decreases as γ_A increases above γ_{AG}; the points (γ_G, γ_{AG}) form the solid curve shown in Fig 6(b). We suggest that for optimal efficacy under MTD constraint, the level of dosage of anti-PD-1 (γ_A) should be related to the level of dosage of GVAX (γ_G) by setting $\gamma_A = \gamma_{AG}$, as indicated by the solid curve in Fig 6(b).

The mathematical model presented in this paper has several limitations:

1. In order to focus on the combined therapy of a cancer vaccine and an anti-PD-1 drug, we did not include some other important cells and cytokines that are found in the tumor microenvironment, such as T regulatory cells, macrophages, endothelial cells, and IL-10, IL-6 and TGF-β. We also did not include blood vessels and oxygen, thus assuming that the tumor is avascular. We tacitly assumed that the effect of these omissions is not significant in comparing the results of therapy to no therapy.
2. We assumed that the densities of immature, or naive, immune cells remain constant throughout the progression of the cancer and that dead cells are quickly removed from the tumor.
3. In estimating parameters we made a steady state assumption in some of the differential equations.
4. In the definition of synergy, and in the synergy map, we included in a crude way the fact that anti-PD-1 causes more toxicity than GVAX. Our aim was to develop a concept that will take account not only of efficacy but also of toxicity. For this reason we compared the treatment benefits for combination (γ_G, γ_A) with the single agents ($2\gamma_G$, 0) and (0, $1.5\gamma_A$).
5. We did not make any direct connection between drugs administered to the patient, and their 'effective strengths' γ_G and γ_A, as they appear in the differential equations, since these data are not available. The order of magnitude of GVAX (10^{-10}) was based on the estimate of the concentration of GM-CSF in normal healthy tissue (see Parameter Estimations for Eq (6)). We simulated the model with different orders of magnitude for anti-PD-1 drug (γ_A) and found the best agreement with the mouse experiments (in Figs 4 and 5) when γ_A is also of order of magnitude 10^{-10}.
6. Although our mathematical model does not presume any geometric form of the tumor, for simplicity, the simulations have been carried out only in the case of a spherical tumor. We note however that spherical cancer models have been used in research as an intermediate between *in vitro* cancer line cultures and *in vivo* cancer [50]. Furthermore, spheroids mirror the 3D cellular context and therapeutically relevant pathophysiological gradient of *in vivo* tumors [51].

Clinical data on efficacy and toxicity are quite limited at this time. Our model should be viewed as setting up a computational framework, to address the question of optimal efficacy in combination therapy with cancer vaccine and checkpoint inhibitor.

Materials and methods

Parameter estimation

Half-saturation. In an expression of the form $Y\frac{X}{K_X+X}$ where Y is activated by X, the half-saturation parameter K_X is taken to be the approximate steady state concentration of species X.

Diffusion coefficients. By [52], we have the following relation for estimating the diffusion coefficients of a protein p:

$$\delta_p = \frac{M_V^{1/3}}{M_p^{1/3}}\delta_V,$$

where M_V and δ_V are respectively the molecular weight and diffusion coefficient of VEGF, M_p is the molecular weight of p, and M_V = 24kDa [53] and $\delta_V = 8.64 \times 10^{-2}$ cm^2 day^{-1} [54]. Since M_{I_2} = 15.5kDa, $M_{I_{12}}$ = 70kDa, M_G = 16.2kDa [55] and M_A = 32kDa [56], we get δ_{I_2} =

9.9956×10^{-2} cm^2 day^{-1}, $\delta_{I_{12}} = 6.0472 \times 10^{-2}$ cm^2 day^{-1}, $\delta_G = 9.8495 \times 10^{-2}$ cm^2 day^{-1}, and $\delta_A = 7.85 \times 10^{-2}$ cm^2 day^{-1}.

Eq (2): The number of DCs in various organs (heart, kidney, pancreas and liver) in mouse varies from 1.1×10^6 cells/cm^3 to 6.6×10^6 cells/cm^3 [57]. Mature DCs are approximately 10 to 15 μm in diameter [58]. Accordingly, we estimate steady states of DCs by $K_D = 4 \times 10^{-4}$ g/cm^3. We assume that the density of immature DCs is smaller than the actived DCs, and take $D_0 = \frac{1}{20} K_D = 2 \times 10^{-5}$ g/cm^3. We also assume that the activation of DCs by GM-CSF-secreting vaccine is more effective than their activation by NCs-secreted HMGB-1, and take $\lambda_{DG} \frac{G}{K_G+G} = 10\lambda_{DC} \frac{C}{K_C+C}$. From the steady state of Eq (2) in the control case (with no drug), we get

$$\lambda_{DC} D_0 \cdot \frac{C}{K_C + C} + \lambda_{DG} D_0 \cdot \frac{G}{K_G + G} - d_D D = 0,$$

where $d_D = 0.1$/day [59], $D_0 = 2 \times 10^{-5}$ g/cm^3, $D = K_D = 4 \times 10^{-4}$ g/cm^3, $C = K_C = 0.4$ g/cm^3, and $G = \hat{K}_G = 1.74 \times 10^{-10}$ g/cm^3 and $K_G = 1.74 \times 10^{-9}$ g/cm^3 ($\hat{K}_G$ and K_G are estimated together with other estimates of Eq (6)). Hence $\lambda_{DC} = 0.364$/day and $\lambda_{DG} = 20.02$/day.

Eq (3): The number of lymphocytes is approximately twice the number of DCs [57]. T cells are approximately 14 to 20 μm in diameter. Assuming that the number of Th1 cells is 1/4 of the number of lymphocytes, we estimate the steady state density of Th1 cells by $K_T = 2 \times 10^{-3}$ g/cm^3. We assume the density of naive CD4$^+$ T cells to be less than the density of Th1, and take $T_{10} = \frac{1}{5} K_T = 4 \times 10^{-4}$ g/cm^3. We also assume that in steady state, $Q/K_{TQ} = 2$ (K_{TQ} is estimated together with other estimates of Eqs (9)–(12)). From the steady state of Eq (3), we get

$$\left(\lambda_{T_1 I_{12}} T_{10} \cdot \frac{1}{2} + \lambda_{T_1 I_2} T_1 \cdot \frac{1}{2}\right) \cdot \frac{1}{3} - d_{T_1} T_1 = 0,$$

where $T_{10} = 4 \times 10^{-4}$ g/cm^3, $T_1 = K_{T_1} = 2 \times 10^{-3}$ g/cm^3, and, by [59], $\lambda_{T_1 I_2} = 0.25$/day and $d_{T_1} = 0.197$/day. Hence $\lambda_{T_1 I_{12}} = 4.66$/day.

Eq (4): The CD4/CD8 ratio in the blood is 2:1. We assume a similar ratio in the tissue, and take $T_{80} = \frac{1}{2} T_{10} = 2 \times 10^{-4}$ g/cm^3. We also take the steady state of T_8 to be half of the steady state of T_1, i.e., $K_{T_8} = \frac{1}{2} K_{T_1} = 1 \times 10^{-3}$ g/cm^3. From the steady state equation of Eq (4), we get

$$\left(\lambda_{T_8 I_{12}} T_{80} \cdot \frac{1}{2} + \lambda_{T_8 I_2} T_8 \cdot \frac{1}{2}\right) \cdot \frac{1}{3} - d_{T_8} T_8 = 0,$$

where $T_{80} = 5 \times 10^{-5}$ g/cm^3, $T_8 = K_{T_8} = 1 \times 10^{-3}$ g/cm^3, and, by [59], $\lambda_{T_8 I_2} = 0.25$/day and $d_{T_8} = 0.18$/day. Hence $\lambda_{T_1 I_{12}} = 4.15$/day.

Eq (5): We take $d_C = 0.17$ day^{-1} and $C_M = 0.8$ g/cm^3 [59]. In the absence of immune responses and anti-tumor drugs, the tumor grows according to

$$\frac{dC}{dt} = \lambda_C C\left(1 - \frac{C}{C_M}\right) - d_C C, \tag{20}$$

and with immune response, the tumor grows according to

$$\frac{dC}{dt} = \lambda_C C\left(1 - \frac{C}{C_M}\right) - (\eta_1 T_1 + \eta_8 T_8) C - d_C C. \tag{21}$$

Mouse experiments show that the tumor volume on average doubles within 5-15 days [21–23]. Assuming a linear growth

$$\frac{dC}{dt} = \lambda_0 C, \quad \text{where } \lambda_0 > 0,$$

during the volume doubling time, we conclude from Eq (21) that

$$\lambda_C C\left(1 - \frac{C}{C_M}\right) - (\eta_1 T_1 + \eta_8 T_8)C - d_C C = \lambda_0 C. \tag{22}$$

where $\lambda_0 \in \left(\frac{\ln 2}{15}, \frac{\ln 2}{5}\right)$. We assume that with no immune responses

$$\frac{dC}{dt} = 2\lambda_0 C,$$

so that, by Eq (20), we get

$$\lambda_C C\left(1 - \frac{C}{C_M}\right) - d_C C = 2\lambda_0 C. \tag{23}$$

We take $\lambda_0 = 0.069$/day, and assume that in steady state of Eqs (20) and (21), C is approximately 0.4 g/cm^3, so that from Eq (23) we get

$$\frac{1}{2}\lambda_C - d_C = 2\lambda_0,$$

or $\lambda_C = 0.616$/day. From Eqs (23) and (22), we get $\eta_1 T_1 + \eta_8 T_8 = \lambda_0$. Noting that T_8 cells kill cancer cells more effectively than T_1 cells, we take $\eta_8 = 4\eta_1$, so that $\eta_1 = \frac{\lambda_0}{T_1 + 4T_8} = 11.5$ cm^3/g · day and $\eta_8 = 46$ cm^3/g · day (with $T_1 = K_{T_1} = 2 \times 10^{-3}$ g/cm^3 and $T_8 = K_{T_8} = 1 \times 10^{-3}$ g/cm^3 as in the estimates for Eqs (3) and (4)).

Eq (6): With no drugs, the steady state plasma concentration of GM-CSF is $G = \hat{K}_G = 1.74 \times 10^{-10}$ g/cm^3 [60]. The half-life of GM-CSF is 13 hours [61], i.e, 0.54 day, so that $d_G = \frac{\ln 2}{0.54} = 1.28$/day. From the steady state of Eq (6) (with no drugs), we get $\lambda_G = d_G G = d_G \hat{K}_G = 2.23 \times 10^{-10}$ g/cm^3 · day. But when the GM-CSF-secreting vaccine is administered, the concentration of GM-CSF shoots up, and we assume that at steady states it reaches the level of $G = K_G = 10\hat{K}_G = 1.74 \times 10^{-9}$ g/cm^3.

Eq (7): From the steady state of Eq (7), we get $\lambda_{I_{12}D} D - d_{I_{12}} I_{12} = 0$, where $d_{I_{12}} = 1.38$/day [59] and $I_{12} = K_{I_{12}} = 1.5 \times 10^{-10}$ g/cm^3 [59], and $D = K_D = 4 \times 10^{-4}$ g/cm^3. Hence, $\lambda_{I_{12}D} = 5.18 \times 10^{-7}$/day.

Eq (8): From the steady state of Eq (8), we get $\lambda_{I_2 T1} T_1 - d_{I_2} I_2 = 0$, where $d_{I_2} = 2.376$/day [59] and $I_2 = K_{I_2} = 2.37 \times 10^{-11}$ g/cm^3 [59], and $T_1 = K_{T_1} = 2 \times 10^{-3}$ g/cm^3. Hence, $\lambda_{I_2 T1} = 2.82 \times 10^{-8}$/day.

Eqs (9)–(12): In order to estimate the parameter K_{TQ} (in Eqs (3) and (4)), we need to determine the steady state concentrations of P and L in the control case (no drugs). To do that, we need to estimate ρ_P and ρ_L. By [62], the mass of one PD-1 protein is $m_P = 8.3 \times 10^{-8}$ pg $= 8.3 \times 10^{-20}$ g, and by [63] the mass of one PD-L1 is $m_L = 5.8 \times 10^{-8}$ pg $= 5.8 \times 10^{-20}$ g. We assume that the mass of one T cell is $m_T = 10^{-9}$ g. By [14], there are 3000 PD-1 proteins and 9000 PD-L1 proteins on one T cell (T_1 or T_8). Since $\rho_P T$ is the density of PD-1 (without anti-PD-1 drug), we get $\rho_P = 3000 \times \frac{m_P}{m_T} = \frac{3000 \times (8.3 \times 10^{-20})}{10^{-9}} = 2.49 \times 10^{-7}$ and $\rho_L = 9000 \times \frac{m_L}{m_T} = \frac{9000 \times (5.8 \times 10^{-20})}{10^{-9}} = 5.22 \times 10^{-7}$.

In steady state, $T_1 = 2 \times 10^{-3}$ g/cm^3 and $T_8 = 1 \times 10^{-3}$ g/cm^3. Hence, in steady state,

$$P = \rho_P(T_1 + T_8) = (2.49 \times 10^{-7}) \times (2 \times 10^{-3} + 1 \times 10^{-3}) = 7.47 \times 10^{-10} \text{ g/ cm}^3.$$

The parameter ε in Eq (10) depends on the type of cancer; many cancer cells, but not all, express PD-L1 [17, 35–37]. Accordingly, we assume ε varies in the interval 0-0.01, but in the simulations we take $\varepsilon = 0.01$. Then, from Eq (10), we get

$$\begin{aligned} L &= \rho_L(T_1 + T_8 + \varepsilon C) = (5.22 \times 10^{-7}) \times [2 \times 10^{-3} + 1 \times 10^{-3} + 0.01 \times 0.4] \\ &= 3.654 \times 10^{-9} \text{ g/ cm}^3. \end{aligned}$$

In steady state with $P = \bar{P}$, $L = \bar{L}$ and $Q = \bar{Q}$, we have, by Eq (12), $\bar{Q} = \sigma \bar{P} \bar{L}$. We take $K_{TQ} = \frac{1}{2}\bar{Q} = \frac{1}{2}\sigma \bar{P}\bar{L}$. Hence, $Q/K_{TQ} = PL/\left(\frac{1}{2}\bar{P}\bar{L}\right)$ and

$$\frac{1}{1 + Q/K_{TQ}} = \frac{1}{1 + PL/\left(\frac{1}{2}\bar{P}\bar{L}\right)} = \frac{1}{1 + PL/K'_{TQ}},$$

where $K'_{TQ} := \frac{1}{2}\bar{P}\bar{L} = \frac{1}{2} \times (7.47 \times 10^{-10}) \times (3.654 \times 10^{-9}) = 1.365 \times 10^{-18}$ g^2/cm^6.

Eq (13): By [42], the half-life of anti-PD-1 is 15 days, so that $d_A = \frac{\ln 2}{15} = 4.62 \times 10^{-2}$ day^{-1}. We assume that 10% of A is used in blocking PD-1, while the remaining 90% degrades naturally. Hence, in steady state, $\mu_{PA}PA/10\% = d_A A/90\%$, so that

$$\mu_{PA} = \frac{d_A}{9P} = \frac{4.62 \times 10^{-2}}{9 \times (7.47 \times 10^{-10})} = 6.87 \times 10^6 \text{ cm}^3/\text{ g} \cdot \text{ day}.$$

If the percentage of A used in blocking PD-1 is changed, the value of μ_{PA} will also change, but the results of simulations do not change qualitatively (not shown here).

Sensitivity analysis

We performed sensitivity analysis, with respect to the tumor radius R at day 60, with respect to some of the production parameters of the System (2)–(13), namely, λ_{DC}, λ_{DG}, $\lambda_{T_1 I_{12}}$, $\lambda_{T_1 I_2}$, $\lambda_{T_8 I_{12}}$, $\lambda_{T_8 I_2}$, and the important parameters K_{TQ}, η_1 and η_8. Following the method in [64], we performed Latin hypercube sampling and generated 1000 samples to calculate the partial rank correlation coefficients (PRCC) and the p-values with respect to the tumor radius at day 60. In sampling all the parameters, we took the range of each from 1/2 to twice its values in Tables 2 and 3. The results are shown in Fig 8.

Not surprisingly all the parameters are negatively correlated with the tumor radius. We note that the highest negatively correlated parameters are the activation rate of dendritic cells by cancer cells (λ_{DC}) and the inhibition of T cells activation by PD-1-PD-L1 complex (K_{TQ}). However, with different values of γ_G and γ_A the parameter λ_{DG} can exceed λ_{DC}.

Computational method

We employ moving mesh method [34] to numerically solve the free boundary problem for the tumor proliferation model. To illustrate this method, we take Eq (2) as example and rewrite it as the following form:

$$\frac{\partial D(r,t)}{\partial t} = \delta_D \Delta D(r,t) - div(\mathbf{u}D) + F, \tag{24}$$

where F represents the term in the right hand side of Eq (2). Let r_i^k and D_i^k denote numerical approximations of i-th grid point and $D(r_i^k, n\tau)$, respectively, where τ is the size of time-step.

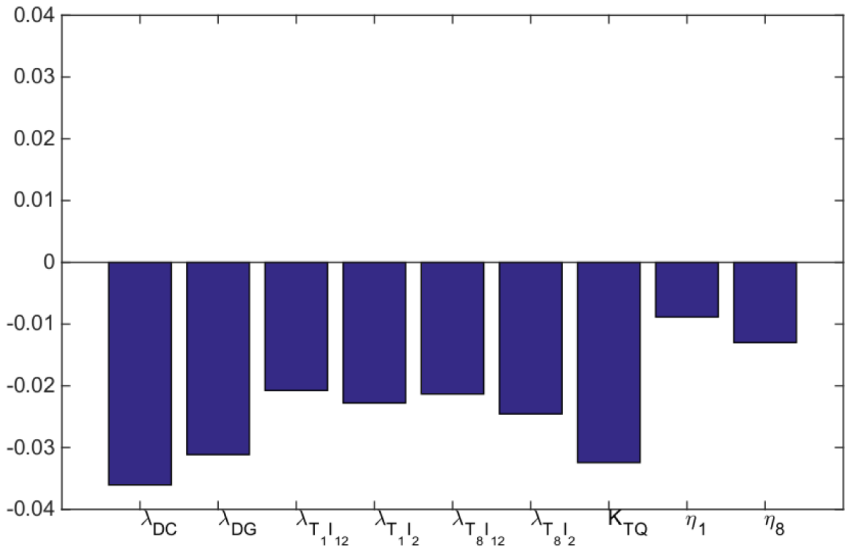

Fig 8. Statistically significant PRCC values (p-value < 0.01) for *R*(*t*) at day 60.

https://doi.org/10.1371/journal.pone.0178479.g008

The discretization of Eq (24) is derived by the fully implicit finite difference scheme:

$$\frac{D_i^{k+1}-D_i^k}{\tau}=\delta_D\left(D_{rr}+\frac{2}{r_i^k}D_r\right)-\left(\frac{2}{r_i^{k+1}}u_i^{k+1}+u_r\right)D_i^{k+1}-u_i^{k+1}D_r+F_i^{k+1}, \tag{25}$$

where $D_r=\frac{h_{-1}^2D_{i+1}^{k+1}-h_1^2D_{i-1}^{k+1}-(h_1^2-h_{-1}^2)D_i^{k+1}}{h_1(h_{-1}^2-h_1h_{-1})}$, $D_{rr}=2\frac{h_{-1}D_{i+1}^{k+1}-h_1D_{i-1}^{k+1}+(h_1-h_{-1})D_i^{k+1}}{h_1(h_1h_{-1}-h_{-1}^2)}$,
$u_r=\frac{h_{-1}^2u_{i+1}^{k+1}-h_1^2u_{i-1}^{k+1}-(h_1^2-h_{-1}^2)u_i^{k+1}}{h_1(h_{-1}^2-h_1h_{-1})}$, $h_{-1}=r_{i-1}^{k+1}-r_i^{k+1}$ and $h_1=r_{i+1}^{k+1}-r_i^{k+1}$. The mesh moves by $r_i^{k+1}=r_i^k+u_i^{k+1}\tau$, where u_i^{k+1} is solved by the velocity equation.

Acknowledgments

This work is supported by the Mathematical Biosciences Institute and the National Science Foundation (Grant DMS 0931642), and the Renmin University of China and the International Postdoctoral Exchange Fellowship Program 2016 by the Office of China Postdoctoral Council.

Author Contributions

Conceptualization: AF XL.

Data curation: AF XL.

Formal analysis: AF XL.

Funding acquisition: AF.

Investigation: AF XL.

Methodology: AF XL.

Project administration: AF XL.

Resources: AF XL.

Software: AF XL.

Validation: AF XL.

Visualization: AF XL.

Writing – original draft: AF XL.

Writing – review & editing: AF XL.

References

1. Sims GP, Rowe DC, Rietdijk ST, Herbst R, Coyle AJ. HMGB1 and RAGE in inflammation and cancer. Annu Rev Immunol. 2010; 28:367–388. https://doi.org/10.1146/annurev.immunol.021908.132603
2. Palucka J, Banchereau J. Cancer immunotherapy via dendritic cells. Nat Rev Cancer. Mar 2012; 12 (4):265–277. https://doi.org/10.1038/nrc3258
3. Saenz R, Futalan D, Leutenez L, Eekhout F, Fecteau JF, Sundelius S, et al. TLR4-dependent activation of dendritic cells by an HMGB1-derived peptide adjuvant. J Transl Med. Aug 2014; 12(211):1–11.
4. Janco JMT, Lamichhane P, Karyampudi L, Knutson KL. Tumor-infiltrating dendritic cells in cancer pathogenesis. J Immunol. Apr 2015; 194(7):2985–2991. https://doi.org/10.4049/jimmunol.1403134
5. Ma Y, Shurin GV, Peiyuan Z, Shurin MR. Dendritic Cells in the Cancer Microenvironment. J Cancer. 2013; 4(1):36–44. https://doi.org/10.7150/jca.5046
6. Fernandez NC, Lozier A, Flament C, Ricciardi-Castagnoli P, Bellet D, Suter M, et al. Dendritic cells directly trigger NK cell functions: cross-talk relevant in innate anti-tumor immune responses in vivo. Nat Med. Apr 1999; 5(4):405–411. https://doi.org/10.1038/7403
7. Gong J, Avigan D, Chen D, Wu Z, Koido S, Kashiwaba M, et al. Activation of antitumor cytotoxic T lymphocytes by fusions of human dendritic cells and breast carcinoma cell. J Cancer. 2000; 97(6):2715–2718.
8. Mailliard RB, Bykovskaya SEQCAKSN, Lotze MT, et al. Complementary dendritic cell-activating function of CD8+ and CD4+ T cells: helper role of CD8+ T cells in the development of T helper type 1 responses. J Exp Med. Feb 2002; 195(4):473–483. https://doi.org/10.1084/jem.20011662
9. Haabeth OAW, Tveita AA, Fauskanger M, Schjesvold F, Lorvik KB, Hofgaard PO, et al. How Do CD4 (+) T Cells Detect and Eliminate Tumor Cells That Either Lack or Express MHC Class II Molecules? Front Immunol. April 2014; 5(174):1–13.
10. van der Burg SH, Arens R, Ossendorp F, van Hall T, Melief CJM. Vaccines for established cancer: overcoming the challenges posed by immune evasion. Nature Reviews Cancer. Mar 2016; 16:219–233. https://doi.org/10.1038/nrc.2016.16
11. Kaufman HL, Ruby CE, Hughes T, Slingluff CLJ. Current status of granulocyte-macrophage colony-stimulating factor in the immunotherapy of melanoma. J Immunother Cancer. May 13, 2014; 2(11):1–13.
12. Gupta R, Emens LA. GM-CSF-secreting vaccines for solid tumors: moving forward. Discov Med. Jul 2010; 10(50):52–60.
13. Simmons AD, Li B, Gonzalez-Edick M, Lin C, Moskalenko M, Du T, et al. GM-CSF-secreting cancer immunotherapies: preclinical analysis of the mechanism of action. Cancer Immunol Immunother. Oct, 2007; 56(10):1653–1665. https://doi.org/10.1007/s00262-007-0315-2
14. Cheng X, Veverka V, Radhakrishnan A, Waters LC, Muskett FW, Morgan SH, et al. Structure and interactions of the human programmed cell death 1 receptor. J Biol Chem. Apr 2013; 288(17):11771–11785. https://doi.org/10.1074/jbc.M112.448126
15. Shi L, Chen S, Yang L, Li Y. The role of PD-1 and PD-L1 in T-cell immune suppression in patients with hematological malignancies. J Hematol Oncol. Sep 2013; 6(74).
16. Muppidi MR, George S. Immune Checkpoint Inhibitors in Renal Cell Carcinoma. Journal of Targeted Therapies in Cancer 2015. 2015; 4:47–52.
17. He J, Hu Y, Hu M, Li B. Development of PD-1/PD-L1 Pathway in Tumor Immune Microenvironment and Treatment for Non-Small Cell Lung Cancer. Scientific Reports. Aug 2015; 5(13110).
18. Kleponis J, Skelton R, Zheng L. Fueling the engine and releasing the break: combinational therapy of cancer vaccines and immune checkpoint inhibitors. Cancer Biol Med. Sep 2015; 12(3):201–208.
19. Guo C, Manjili MH, Subjeck JR, Sarkar D, Fisher PB, et al. Therapeutic Cancer Vaccines: Past, Present and Future. Adv Cancer Res. 2013; 119:421–475. https://doi.org/10.1016/B978-0-12-407190-2.00007-1

20. Burotto M, Singh N, Heery CR, Gulley JL, Mada RA. Exploiting synergy: immune-based combinations in the treatment of prostate cancer. Front Oncol. December 12, 2014; 4(351):1–10.
21. Ali OA, Lewin SA, Dranoff G, Mooney DJ. Vaccines combined with immune checkpoint antibodies promote cytotoxic T cell activity and tumor eradication. Cancer Immunology Research. Dec 15, 2015; p.
22. Tian H, Shi G, Wang Q, Li Y, Yang Q, Li C, et al. A novel cancer vaccine with the ability to simultaneously produce anti-PD-1 antibody and GM-CSF in cancer cells and enhance Th1-biased antitumor immunity. Signal Transduction and Targeted Therapy. October 15, 2016; 1(16025).
23. Li B, VanRoey M, Wang C, hui Timothy Chen T, Korman A, Jooss K. Anti-programmed death-1 synergizes with granulocyte macrophage colony-stimulating factor-secreting tumor cell immunotherapy providing therapeutic benefit to mice with established tumors. Clin Cancer Res. 2009; 15(5):1623–1634. https://doi.org/10.1158/1078-0432.CCR-08-1825
24. Soares KC, Rucki AA, Wu AA, Olino K, Xiao Q, Chai Y, et al. PD-1/PD-L1 blockade together with vaccine therapy facilitates effector T-cell infiltration into pancreatic tumors. J Immunother. Jan 2015; 38 (1):1–11. https://doi.org/10.1097/CJI.0000000000000062
25. Fu J, Malm IJ, Kadayakkara DK, Levitsky H, Pardoll D, Kim YJ. Preclinical evidence that PD1 blockade cooperates with cancer vaccine TEGVAX to elicit regression of established tumors. Cancer Res. Aug 1, 2014; 74(15):4042–4052. https://doi.org/10.1158/0008-5472.CAN-13-2685
26. Rosenblatt J, Glotzbecker B, Mills H, Vasir B, Tzachanis D, Levine JD, et al. PD-1 blockade by CT-011, anti PD-1 antibody, enhances ex-vivo T cell responses to autologous dendritic/myeloma fusion vaccine. J Immunother. Jun 2011; 34(5):409–418. https://doi.org/10.1097/CJI.0b013e31821ca6ce
27. Duraiswamy J, Kaluza KM, Freeman GJ, Coukos G. Dual blockade of PD-1 and CTLA-4 combined with tumor vaccine effectively restores T-cell rejection function in tumors. Cancer Res. June 15, 2013; 73 (12):3591–3603. https://doi.org/10.1158/0008-5472.CAN-12-4100
28. Serre R, Benzekry S, Padovani L, Meille C, Nicolas Andre JC, et al. Mathematical Modeling of Cancer Immunotherapy and Its Synergy with Radiotherapy. Cancer Res. September 2016; 76(17):4931–40. https://doi.org/10.1158/0008-5472.CAN-15-3567
29. Joshi B, Wang X, Banerjee S, Tian H, Matzavinos A, Chaplain MAJ. On immunotherapies and cancer vaccination protocols: a mathematical modelling approach. J Theor Biol. Aguest 2009; 259(4):820–827. https://doi.org/10.1016/j.jtbi.2009.05.001
30. vG de Pillis L, Gu W, Radunskay AE. Mixed immunotherapy and chemotherapy of tumors: modeling, applications and biological interpretations. J Theor Biol. February 2006; 238(4):841–862. https://doi.org/10.1016/j.jtbi.2005.06.037
31. Zandarashvili L, Sahu D, Lee K, Lee YS, Singh P, Rajarathnam K, et al. Real-time kinetics of high-mobility group box 1 (HMGB1) oxidation in extracellular fluids studied by in situ protein NMR spectroscopy. J Biol Chem. April 2013; 288(17):11621–11627. https://doi.org/10.1074/jbc.M113.449942
32. van de Laar L, Coffer PJ, Woltman AM. Regulation of dendritic cell development by GM-CSF: molecular control and implications for immune homeostasis and therapy. Blood. April 2012; 119(15):3383–3393. https://doi.org/10.1182/blood-2011-11-370130
33. Mautea RL, Gordona SR, Mayere AT, McCrackena MN, Natarajane A, Ring NG, et al. Engineering high-affinity PD-1 variants for optimized immunotherapy and immuno-PET imaging. Proc Natl Acad Sci USA. Nov 2015; 112(47):E6506–14. https://doi.org/10.1073/pnas.1519623112
34. D'Acunto B. Computational Methods for PDE in mechanics. Series on Advances in Mathematics for Applied Sciences-Vol.67. Singapore: Word Scientific; 2004.
35. Buttea MJ, Pena-Cruzc V, Kima MJ, Freemanc GJ, Sharpe AH. Interaction of human PD-L1 and B7-1. Mol Immunol. Aug 2008; 45(13):3567–3572. https://doi.org/10.1016/j.molimm.2008.05.014
36. Taube JM, Anders RA, Young GD, Xu H, Sharma R, McMiller TL, et al. Colocalization of inflammatory response with B7-h1 expression in human melanocytic lesions supports an adaptive resistance mechanism of immune escape. Sci Transl Med. March 2012; 4(127):127ra37. https://doi.org/10.1126/scitranslmed.3003689
37. Taube JM, Klein A, Brahmer JR, Xu H, Pan X, Kim JH, et al. Association of PD-1, PD-1 ligands, and other features of the tumor immune microenvironment with response to anti-PD-1 therap. Clin Cancer Res. October 2014; 20(19):5064–5074. https://doi.org/10.1158/1078-0432.CCR-13-3271
38. Jaffee EM, Hruban RH, Biedrzycki B, Laheru D, Schepers K, Sauter PR, et al. Novel allogeneic granulocyte-macrophage colony-stimulating factor-secreting tumor vaccine for pancreatic cancer: a phase I trial of safety and immune activation. J Clin Oncol. 2001; 19:145–156. https://doi.org/10.1200/JCO.2001.19.1.145
39. Laheru D, Lutz E, Burke J, Biedrzycki B, Solt S, Onners B, et al. Allogeneic granulocyte macrophage colony-stimulating factor-secreting tumor immunotherapy alone or in sequence with cyclophosphamide

for metastatic pancreatic cancer: a pilot study of safety, feasibility, and immune activation. Clin Cancer Res. 2008; 14:1455–1463. https://doi.org/10.1158/1078-0432.CCR-07-0371

40. Lutz E, Yeo CJ, Lillemoe KD, Biedrzycki B, Kobrin B, Herman J, et al. A lethally irradiated allogeneic granulocyte-macrophage colony stimulating factor-secreting tumor vaccine for pancreatic adenocarcinoma. A Phase II trial of safety, efficacy, and immune activation. Ann Surg. 2011; 253:328–335. https://doi.org/10.1097/SLA.0b013e3181fd271c

41. Hamid O, Robert C, Daud A, Hodi FS, Hwu WJ, Kefford R, et al. Safety and tumor responses with lambrolizumab (anti-PD-1) in melanoma. N Engl J Med. 2013; 369:134–44. https://doi.org/10.1056/NEJMoa1305133

42. Brahmer JR, Drake CG, Wollner I, Powderly JD, Picus J, Sharfman WH, et al. Phase I study of single-agent anti-programmed death-1 (MDX-1106) in refractory solid tumors: safety, clinical activity, pharmacodynamics, and immunologic correlates. J Clin Oncol. 2010; 28:3167–3175. https://doi.org/10.1200/JCO.2009.26.7609

43. Topalian SL, Hodi FS, Brahmer JR, Gettinger SN, Smith DC, McDermott DF, et al. Safety, activity, and immune correlates of anti-PD-1 antibody in cancer. N Engl J Med. 2012; 366:2443–2454. https://doi.org/10.1056/NEJMoa1200690

44. Swart M, Verbrugge I, Beltman JB. Combination Approaches with Immune-Checkpoint Blockade in Cancer Therapy. Front Oncol. 2016; 6(233):1–16.

45. Soares KC, Rucki AA, Wu AA, Olino K, Xiao Q, Chai Y, et al. PD-1/PD-L1 blockade together with vaccine therapy facilitates effector T-cell infiltration into pancreatic tumors. J Immunother. 2015; 38(1):1–11. https://doi.org/10.1097/CJI.0000000000000062

46. Owonikoko TK, Ramalingam SS. Minimize toxicity or preserve efficacy? A delicate trade-off in the management of older patients with lung cancer. J Clin Oncol. February 2015; 33(6):534–536. https://doi.org/10.1200/JCO.2014.59.5033

47. Lee CK, Gebski VJ, Coates AS, Veillard AS, Harvey V, Tattersall MH, et al. Trade-offs in quality of life and survival with chemotherapy for advanced breast cancer: mature results of a randomized trial comparing single-agent mitoxantrone with combination cyclophosphamide, methotrexate, 5-fluorouracil and prednisone. Springerplus. Augest 2013; 21(391):1–10.

48. Marshall DA, Deal K, Bombard Y, Leighl N, MacDonald KV, Trudeau M. How do women trade-off benefits and risks in chemotherapy treatment decisions based on gene expression profiling for early-stage breast cancer? A discrete choice experiment. BMJ Open. June 2016; 6(6):e010981. https://doi.org/10.1136/bmjopen-2015-010981

49. Blinman P, King M, Norman R, Viney R, Stockler MR. Preferences for cancer treatments: an overview of methods and applications in oncology. Ann Oncol. 2012; 23(5):1104–1110. https://doi.org/10.1093/annonc/mdr559

50. Weiswald LB, Bellet D, Dangles-Marie V. Spherical cancer models in tumor biology. Neoplasia. 2015; 17(1):1–15. https://doi.org/10.1016/j.neo.2014.12.004

51. Hirschhaeuser F, Menne H, Dittfeld C, West J, Mueller-Klieser W, Kunz-Schughart LA. Multicellular tumor spheroids: An underestimated tool is catching up again. J Biotechnol. 2010; 148(1):3–15. https://doi.org/10.1016/j.jbiotec.2010.01.012

52. Young ME. Estimation of diffusion coefficients of proteins. Biotechnology and Bioengineering. 1980; XXII:947–955. https://doi.org/10.1002/bit.260220504

53. Shui YB, Wang X, Hu JS, Wang SP, Garcia CM, et al. Vascular endothelial growth factor expression and signaling in the lens. Invest Ophthalmol Vis Sci. 2003; 44(9):3911–3919. https://doi.org/10.1167/iovs.02-1226

54. Liao KL, Bai XF, Friedman A. Mathematical modeling of interleukin-27 induction of anti-tumor T cells response. PLoS ONE. 2014; 9(3):e91844. https://doi.org/10.1371/journal.pone.0091844

55. PhosphoSitePlus/. GM-CSF, http://www.phosphosite.org/proteinAction?id=2454248&showAllSites = true;

56. Abcam/. Anti-PD1 antibody (ab89828), http://www.abcam.com/pd1-antibody-ab89828.html;

57. Steptoe RJ, Patel RK, Subbotin VM, Thomson AW. Comparative analysis of dendritic cell density and total number in commonly transplanted organs: morphometric estimation in normal mice. Transpl Immunol. 2000; 8(1):49–56. https://doi.org/10.1016/S0966-3274(00)00010-1 PMID: 10834610

58. Dumortier H, van Mierlo GJD, Egan D, van Ewijk W, Toes REM, Offringa R, et al. Antigen presentation by an immature myeloid dendritic cell line does not cause CTL deletion in vivo, but generates CD8+ central memory-like T cells that can be rescued for full effector function. J Immunol. 2005; 175(2):855–863. https://doi.org/10.4049/jimmunol.175.2.855 PMID: 16002683

59. Hao W, Friedman A. The role of exosomes in pancreatic cancer microenvironment. Bull Math Biol. 2017;accepted.

60. Fiehn C, Wermann M, Pezzutto A, Hufner M, Heilig B. Plasma GM-CSF concentrations in rheumatoid arthritis, systemic lupus erythematosus and spondyloarthropathy. Z Rheumatol. 1992; 51(3):121–126. PMID: 1502858

61. Dale DC, Liles WC, Llewellyn C, Price TH. Effects of granulocyte-macrophage colony-stimulating factor (GM-CSF) on neutrophil kinetics and function in normal human volunteers. Am J Hematol. 1998; 57 (1):7–15. https://doi.org/10.1002/(SICI)1096-8652(199801)57:1%3C7::AID-AJH2%3E3.0.CO;2-0 PMID: 9423810

62. Agata Y, Kawasaki A, Nishimura H, Ishida Y, Tsubat T, Yagita H, et al. Expression of the PD-1 antigen on the surface of stimulated mouse T and B lymphocytes. Int Immunol. 1996; 8(5):765–772. https://doi.org/10.1093/intimm/8.5.765 PMID: 8671665

63. Human PD-L1/B7-H1/CD274 Protein. Sino Biological Inc, http://wwwsinobiologicalcom/PD-L1-B7-H1-CD274-Protein-g-533html;

64. Marino S, Hogue I, Ray C, Kirschner D. A methodology for performing global uncertainty and sensitivity analysis in systems biology. J Theor Biol. 2008; 254(1):178–196. https://doi.org/10.1016/j.jtbi.2008.04.011 PMID: 18572196

65. Hao W, Schlesinger LS, Friedman A. Modeling Granulomas in Response to Infection in the Lung. PLoS ONE. March 17, 2016; 11(3):e0148738. https://doi.org/10.1371/journal.pone.0148738 PMID: 26986986

66. Rini B. Future approaches in immunotherapy. Semin Oncol. Oct 2014; 41(5, Suppl 5):S30–S40. https://doi.org/10.1053/j.seminoncol.2014.09.005 PMID: 25438998